Jurnal Teknologi

Full Paper

MI-OPTNET: AN OPTIMIZED DEEP LEARNING FRAMEWORK FOR MYOCARDIAL INFARCTION DETECTION

Audrey Huong[a]*, Kim Gaik Tay[a], Kok Beng Gan[b], Xavier Ngu[a]

[a]Faculty of Electrical and Electronic Engineering, Universiti Tun Hussein Onn Malaysia, 86400 Batu Pahat, Johor, Malaysia
[b]Faculty of Engineering and Built Environment, Universiti Kebangsaan Malaysia, 43600 UKM Bangi, Selangor, Malaysia

Article history
Received
26 July 2023
Received in revised form
24 November 2023
Accepted
13 December 2023
Published Online
20 April 2024

*Corresponding author
audrey@uthm.edu.my

Graphical abstract

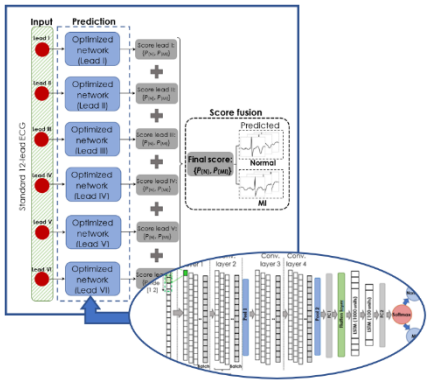

Abstract

The conventional means of myocardial infarction (MI) detection using a 12-lead electrocardiogram (ECG) system include a pretrained network and machine learning interpretation of the complex ECG signals. They are computationally inefficient and demand high-performance hardware. Here, for the first time, we introduce an effective framework (MI-OptNet) using the particle swarm optimization model (PSO) in the design of a lightweight hybrid network combining convolutional neural network (CNN)-long short terms memory (LSTM) for MI and normal ECG detection. We optimized important design and training parameters based on limb leads' signals and identified leads III and VI as the best ECG leads for the task based on their high classification performance ranging between 80 – 90 %, suggesting that they may provide more information about MI than the others. The other strategy of fusing the scores from all models at the decision level achieved the best result with a 10 % increase in the evaluated metrics. Our findings support the flexibility and adaptability of our framework for the design process using minimal computer efforts. We concluded that this approach may be used for other classification problems to assist engineers and designers in efficient decision-making and to solve complex signal classification and recognition problems.

Keywords: Decision Support, myocardial infarction, healthcare, network design, optimization

Abstrak

Kaedah pengesanan infarksi miokardium (MI) menggunakan sistem elektrokardiogram (ECG) 12-elektrod termasuk menggunakan pembelajaran mesin bagi penafsiran isyarat ECG yang kompleks. Teknik ini tidak cekap dari segi keperluan perkakasan komputer berprestasi tinggi. Di sini kami memperkenalkan rangka kerja berkesan (MI-OptNet) menggunakan model pengoptimuman kawanan zarah (PSO) dalam merekabentuk rangkaian hibrid yang menggabungkan CNN dan model LSTM untuk pengesanan MI dan ECG. Kami mengoptimumkan proses reka bentuk dan parameter penting serta mengenalpasti elektrod III dan VI sebagai petunjuk ECG terbaik berdasarkan ketepatan ramalan yang tinggi dalam julat antara 80 – 90 %. Keputusan ini menunjukkan bahawa kedua-dua elektrod ini memberikan lebih banyak maklumat tentang MI daripada yang lain. Strategi lain menggabungkan skor daripada semua model memberikan hasil terbaik dengan peningkatan sebanyak 10% dalam metrik yang dinilai. Penemuan kami menyokong fleksibiliti dan kebolehsuaian rangka kerja kami dalam proses reka bentuk. Kami menyimpulkan bahawa pendekatan ini boleh digunakan untuk masalah pengelasan lain bagi

membantu jurutera dan pereka bentuk dalam membuat keputusan dan menyelesaikan masalah pengelasan isyarat yang kompleks.

Kata kunci: Sokongan Keputusan, infarksi miokardium, penjagaan kesihatan, reka bentuk rangkaian, pengoptimuman

1.0 INTRODUCTION

According to the World Health Organization, cardiovascular disease (CVD) ranks the number one global cause of death in 2019, with acute heart attack, medically known as MI, being a contributory factor [1]. This disease is a serious medical emergency due to tissue necrosis following disruption of blood supply to an area of the myocardium (i.e., myocardial ischemic), causing tissue injury or death. The key factors of MI are hypertension, coronary artery disease, arteriosclerosis, and fatty liver disease. Other causes include the effects of drugs, venom-induced anaphylactic shock, and vasospasm-induced infarction. In addition, cardiovascular complications associated with the Coronavirus Disease 2019 (COVID-19) have been well-documented in recent years. A report by the Centers for Disease Control and Prevention (CDC) in [2] showed evidence of a high prevalence of inflammation of heart muscle (or myocarditis) and pericardium (known as pericarditis) in patients receiving mRNA-based COVID-19 vaccines. Myocarditis is another cause of MI, as the initiation and progression of myocarditis-related inflammation leads to reduced blood flow to the heart muscles. Since the symptoms of MI, which include chest pain or fluttering and pounding heart, are either absent or appear late in the course of the disease [3], it is often referred to as a silent killer. A blood test is a reliable method and early tool to detect cardiac diseases and Heart-type fatty acid-binding protein (h-fabp), a biomarker for MI [4]. However, there is a risk of blood sample contamination in the laboratory. An Electrocardiogram (ECG or EKG) for noninvasive and real-time display of heart signals remains crucial for regular monitoring of heart conditions.

A three-lead ECG is the most basic existing system, whereas a 12-lead ECG is widely used clinically to provide a possible clue to cardiac diseases using the measurement from two sets of ECG leads — limb and chest lead. Limb leads consist of bipolar leads (Lead I, II, and III) and augmented vector leads (i.e., aVR, aVL, aVF). The chest limbs are unipolar cardiac leads, i.e., V1 to V6, positioned on the left side of the chest. The lead configuration of aVR through V6 is described as lead IV - XII. Each lead records heartbeats reflecting conditions of different heart regions, with limb and cardiac leads measuring signals in the vertical and horizontal directions. A normal ECG cycle comprises the P-wave, QRS complex, ST segment, and T wave. The ST segment elevation (i.e., STEMI) or depression (NSTEMI) and intervals related to the R peak have been reported to offer diagnostic information on MI. However, the heart disease-related physiological changes in the PQRST complex can be challenging to detect and interpret by nonspecialists. Furthermore, the waveform can also be easily corrupted by noises, such as power line interference, high-frequency noises, respiratory signals, and motion artifacts, leading to inconclusive diagnoses responsible for over 41 % of failure, delay, and wrong diagnosis [5]. Thus, careful examination of all leads' signals may disclose heart abnormalities and the process demands domain experts with rich experiences. Due to time constraints and difficulties associated with limited experts needing to deal with a large amount of data, machine learning or computer-aided diagnosis (CAD) has become an effective tool to support physicians in their decision-making.

Research related to ECG signal processing in the past dealt with heart disease classification methods [5,6], denoising and filtering methods [7,8], data enhancement techniques [9], biometric recognition [10], and investigations of the telehealth opportunity [11, 12]. Most of these reviewed studies used MIT-BIH Arrhythmia, Physikalisch-Technische Bundesanstalt (PTB), IN-CART, and supraventricular arrhythmias (SV) datasets, downloadable from the PhysioNet website in their investigation. The MIT-BIH and PTB are comparatively famous for use in numerous important publications in the field to benchmark their performance against their competitors. Each database contains 12-lead ECG signals with a different diagnosis. The MI diagnosis is absent in the MIT-BIH database, while PTB published the highest number of this disease before the release of PTB-XL in 2021. A high-class imbalance problem in these datasets is often the case in practice. To overcome this issue, [13] divided a time series signal into multiple cardiac cycles to enrich the training set before extracting their temporal characteristics for analysis. Others in [14] and [15] adopted an innovative strategy to generate data for training deep learning (DL) models using generative adversarial network (GAN)

and synthetic minority oversampling technique (SMOTE). Rai and Chatterjee [15] included the combined dataset of MIT and PTB (normal class) in their investigation. Since a cardiac cycle is sufficient to provide valuable information about heart disease, it has been proposed as a powerful solution to increase data diversity. Several recent efforts have been made toward cardiac cycle extraction. These include [13], where the *ecgpuwave* software is used to segment each wave and annotate the locations of PQRST in ECG signals to determine the temporal features related to the R peak for MI prediction. Another study in [16] explored strategies for detecting QRS complex before extracting a single pulse unit for classifying STEMI and NSTEMI. Śmigiel *et al.* [17] investigated the efficiency of six state-of-the-art detectors for determining the R-peak, which is often taken as the reference point for identifying a single ECG pulse. However, this task can be challenging as the signal is corrupted with noise and baseline wandering. There is also a high intra-patient and inter-patient variability in the PQRST pattern and interval. To this end, some works introduced raw ECG sequences to mitigate the effects of these variations in the training data. This includes Li *et al.* [14], which compared the performance of the GAN model trained using ECG signals of three frame lengths, i.e., 1024, 2048, and 5120. Each window may contain several PQRST complexes or incomplete or truncated ECG segments to predict heart disease.

Transfer learning of CNN is popular among many other scholars in this field. Bassiouni *et al.* [18] compared the learning capacity of ResNet50 trained for feature extraction and MI classification tasks using 2D wavelet transform (ECG images) constructed from 1-dimensional (1D) signals. In [19], the classification of ECG images created from 12-lead signals was performed on ten pretrained networks, including different variants of VGG, ResNet and Inception, MobileNet, Xception, and DenseNet. Gradient-weighted class activation mapping (Grad-CAM) was employed to locate the important regions in the image to differentiate STEMI and NSTEMI signals. The results compared with three state-of-the-art machine learning models, i.e., Support Vector Machine (SVM), K-Nearest Neighbour (KNN), and Decision Tree (DT), showed the superiority of CNNs. Park *et al.* [16] constructed a 1D version of ResNet and VGGNet for the same reasons. Manimekalai and Kavitha [20] used CNN to automatically extract spatial features and LSTM for the temporal component to distinguish between MI and normal beats. A similar study was conducted by [15] to compare the efficiency between CNN and LSTM and a hybrid CNN-LSTM. Al Rahhal *et al.* [13] employed an autoencoder technique for unsupervised learning of features for different classes of ECG waveform: normal, ventricular, supra-ventricular, and the fusion of normal and unknown beats. Unlike the prior works that used the raw ECG signals, Fatimah *et al.* [21] proposed to work on frequency domain statistical features as the input features for their machine learning framework. The manual feature engineering process can be cost-effective in providing good results at a lower computational cost, but it requires expert knowledge pertinent to the system.

Considering the highly complex and dynamic relationship between the ECG pattern and class labels, most of the previous studies relied on pretrained models to learn useful representations of the input ECG data in mapping the input layer-output target relationship. Nonetheless, these models may not be efficient and fully adaptable for the task. Thus, the CNN architecture design and development works were carried out in [17,22,23] to address the classification problem specific to the ECG using the manual approach. The nodes are arranged and positioned in the network by administrator control for reliable and cost-efficient operation. The process can be labor-intensive and time-consuming. These studies focused on recognizing cardiac patterns, i.e., ST/T change and conduction disturbances, which are well-recognized critical features for detecting abnormalities, such as tachycardia and arrhythmias, and MI. Among these diseases, MI is the most dangerous, with the highest mortality rate [24]. To our knowledge, efforts have yet to be made to incorporate an optimization algorithm in designing a deep learning network specific to ECG data. Such work is important to facilitate knowledge discovery, driven by the progressive emergence of new (cardiac) disease datasets, by rapidly and efficiently establishing the complex relationship between the input information and the output. In addition, processing all 12-lead signals may be resource and memory-demanding, so the optimal ECG leads for MI prediction remain to be discovered. Our contributions are three-fold as follows: First, we develop an optimization incorporated system for the systematic and automatic network design process for MI and normal ECG classification. Second, we propose the best ECG lead for MI detection. Third, we improve the decision-making performance by introducing an all-inclusive (i.e., score fusion) strategy.

2.0 METHODOLOGY

2.1 Data Handling and Management

We used the public resource of PTB-XL ECG signals published by the Physical-Technical Federal Institution to demonstrate our proposed framework and investigate our system. It is freely downloadable from PhysioNet's official site (https://physionet.org).

This current largest available database contains 21,837 12-lead ECG signals of five super-classes of diagnoses recorded from 18,885 subjects and their demographic profile. The objective of this study is to classify MI and healthy control. There are 2,685 records with the MI label, while the control dataset consists of 9,528 samples. Each signal is sampled at f_s = 100 Hz. First, we run the *rdsamp* function linked to the waveform database (WFDB) application library to

read the WFDB signal files before inputting its numeric records into MATLAB (version 2022). Each record contains 12 signals from limb and chest (or precordial) electrodes. We intend to establish our diagnosis by examining the limb leads, i.e., lead I through VI, because the signals are similar in all cardiac leads [25], so only the numeric data of limb leads are saved in a mat file for further processing. Next, the signals are applied with a highpass filter of 0.05 Hz to remove baseline drift noise and powerline interference. We used a third-order Butterworth filter for this purpose. We found that using higher order values resulted in large oscillation in the filtered output. Next, we split the data for training, validation, and testing using a ratio of 75 %, 10 %, and 15 % to prevent data leakage. Even though most research acknowledged 80-10-10 % as the standard scheme for data partitioning, studies in [26,27] explored the model predictive performance using different split ratios. While a strict ratio, e.g., 60-30-10 %, renders insufficient training data for learning important features and patterns, a lenient setting like 90-5-5 % lacks rigorous testing of the model. Therefore, the data partitioning scheme adopted herein is chosen after considering a tradeoff between the sufficiency of model training and the robustness of the evaluation to prevent bias in the results. We applied the same seed number to reproduce the data for each run.

2.2 ECG Pulse Segmentation

Each recording of the 10-second ECG filtered signal shown in the second diagram in Figure 1 contains several heart pulses. We truncate the signal according to each heart pulse, and each should be the same length to ensure consistency in the input data fed into the network. We pursued this goal by finding the first maximum of an ECG waveform, and the R-peaks are identified as the points in the signal with amplitudes of at least 95 % of the value. The R peak is used as a reference to centralize PQRST complexes, whereas the duration between two R-peaks, *t*, in Figure 1, is the period of each cycle. The number of heartbeats in each ECG record is estimated by dividing the signal into segments with length *t*. The median cardiac cycle lengths in MI and normal classes are calculated as 0.83 and 0.90 seconds, respectively. A sliding window of 0.83 seconds was used for the entire investigation to eliminate the need for data extrapolation and upsampling during post-processing to match the normal ECG resolution, thereby reducing the computational burden and uncertainty of the estimates. The ECG pulse segmentation process is shown in Figure 1. There are 109,908, 14,664, and 21,984 ECG pulses extracted from training, validation, and test sets.

2.3 Classification Model and Optimized Training Framework

Unlike the existing pretrained CNN models developed for image recognition tasks, we dealt with the 1D-ECG

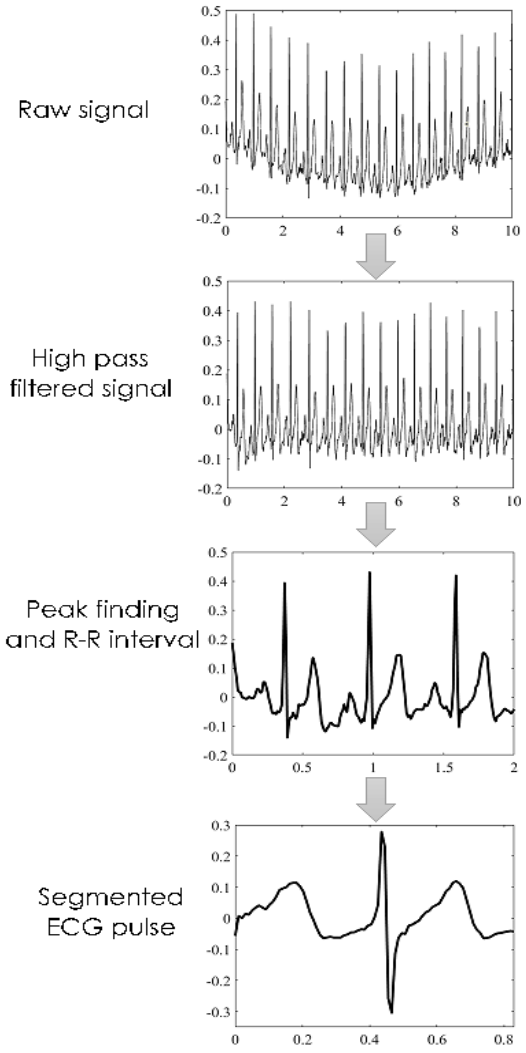

Figure 1 ECG signal preprocessing and segmentation

signal. For this reason, we designed an automatic framework named MI-OptNet, combining an optimization technique and a convolutional-LSTM model for classifying MI and normal ECG signals. The pursuit of this task starts by defining the basic architecture as a hybrid CNN-LSTM to capture both spatial and temporal features in data. The proposed architecture shown in Figure 2 has a uniform structure and is made by stacking convolutional (conv1-conv4) and pooling layers. Once the architecture is fixed, the dimensions of the neural network (i.e., filter and max-pooling sizes and filter numbers) are automatically adjusted via optimization technique for optimal depth estimate and cost-effective operation.

The bounds of the network design-related parameters in Table 1 are chosen based on the ranges used in some of the popular pretrained networks, such as AlexNet, the variants of VGGNet, ResNet, and inceptions. The maximum depth (filter number) of 30 is

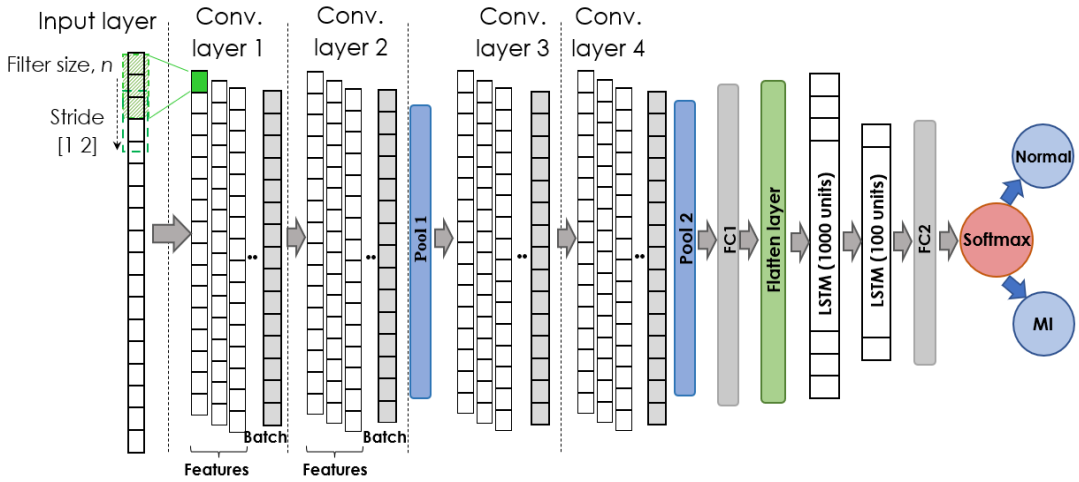

Figure 2 MI-OptNet: Optimization of the hybrid CNN-LSTM architecture design

Table 1 Design and training parameters and their search range

Element	Parameters	Lower bound	Upper bound
Network layers (Conv1-4)	Filter size, *n*	3	10
	Filter number, *N*	8	30
Network layers (Pool 1 and 2)	MaxPooling size, *a*	2	10
Training hyperparameter	Learner type, *L*	{*Adam, Sgdm, RMSProp*}	
	Mini-batch number, *β*	2^3	2^{10}
	Init.learning rate, *γ*	$1e^{-6}$	$1e^{-1}$

considerably smaller than the existing networks because our primary intention is to design a system with practical implementation in mind. This is achieved by designing a lightweight, high-quality model without demanding heavy computer effort. The stride number and the two LSTM hidden units' number in the figure are arbitrarily set as (1 2), 1000, and 100, respectively. The mode of padding is set as 'same'. Apart from the three design parameters mentioned above, important training hyperparameters, namely learner type, mini-batch size, and initial (Init.) learning rate, are also automatically fine-tuned for weight-tuning works to extract the most relevant features for the task.

This setting gives us six degrees of freedom to tune the design parameters using the PSO model. This

Algorithm 1: PSO optimization procedure of network design

Input: Pre-training dataset, swarm size, training, and iteration setting: *Max_iter*, *Max_epoch*, *Max_inc*.
Parameter: Design and training parameters: {*n*, *N*, *a*, *L*, *β*, *γ*}
Output: Global minima position, $\mathbf{P_G} = \{n_G, N_G, a_G, L_G, \beta_G, \gamma_G\}$

Initialize Position in search space, $\mathbf{P_i} = \{n, N, a, L, \beta, \gamma\}$
while iter < *Max_iter* **do**
Training network
if epoch **<** *Max_epoch* **then**
Update network weights by minimizing loss function
Update training & validation accuracies
while val. accuracy increment count < *Max_inc* **do**
Increment epoch count
end while
else
Update last training & validation accuracies & time
Calculate the minimization function in (1)
Identify the current minima
Update position, $\mathbf{P_U} = \{n_U, N_U, a_U, L_U, \beta_U, \gamma_U\}$
end if
Increment iter count
end while
Get global minimum, $\mathbf{P_G} = \{n_G, N_G, a_G, L_G, \beta_G, \gamma_G\}$
return $\mathbf{P_G}$

technique is based on the social behavior of a flock of animals with no leader by following one of the members with the closest position with the potential solution. This method performs better than other optimization techniques, such as genetic algorithm and Bayesian, especially in a high-complexity search space. The flow of the PSO process is shown in Algorithm 1. The process started by launching 20 random points in the defined search space shown in Table 1. Each particle is allowed to iterate 20 times (i.e., *Max_iter* in Algorithm 1). In each iteration, each particle moves around the multidimensional search space, and its position is optimized by minimizing an objective function, $f(A_T, A_V, t)$, given in Eq. (1). The best point is found, updated, and used as the new reference point.

$$f(A_T, A_v, t) = (100 - A_T)^3 + (100 - A_v)^4 + {}^{t}/_{1e^3}. \quad (1)$$

A_T, A_V, and t are training and validation accuracy, and training time, respectively. The point that yields the lowest objective function value is selected as the final solution (i.e., $\boldsymbol{P_G}$ in Algorithm 1). We iterate the process for each ECG lead (Lead I-VI).

The best network design for each lead selected automatically based on training and validation set performances in Eq. (1) is saved for the subsequent evaluations on the test set. In the experiments, we kept the epoch number constant as 100 (i.e., *Max_epoch*) for training each model, leaving the rest of the training parameters other than those optimized in the present study as default. The early stopping criterion is based on the validation performance, i.e., the validation accuracy fails to increase for 50 successive iterations (i.e., *Max_inc*). To address the imbalance class problem, we used weighted entropy loss to assign different weights to the loss of each class. The class weight vector is calculated as the ratio between the training data size and class frequency as 4.6 and 1.3, respectively, for MI and normal labels. Another effort to reduce model overfitting is using a dropout regularization rate of 0.2 after each LSTM layer in Figure 2.

2.4 Limb-Lead Networks and All-Inclusive System Framework

There is variation in ECG signals from the examined limb leads as each explores a different heart region. Some lead signals may provide more useful information on MI events than others, and there is no golden standard on the best ECG lead for monitoring MI. In medical practice, medical professionals carefully assessed and examined all lead signals in their diagnosis. Their clinical importance has also prompted researchers in the computer vision domain to consider standard 12-lead ECG signals in their analysis. However, this is at the price of higher computational time and resources.

We used signals from the bipolar (lead I, II, and III) and unipolar limb leads (lead IV, V, and VI) in our processing and analysis to lessen the computing power. The search process from section 2.3 gives us six models optimized and used independently for predicting signals from each lead, as shown in Figure 3. Hence, different lead networks may produce different diagnoses in the testing phase. We take this effort to the next level by adopting an all-inclusive system combining the probability for MI and normal classes from each network, represented by $P_{(MI)}$ and $P_{(N)}$ in the figure. These outputs were fused by direct summing their values to provide further confidence in the result. The target class with the higher total score from the score fusion process (i.e., Fusion MI-OptNet) is chosen as the final predicted label.

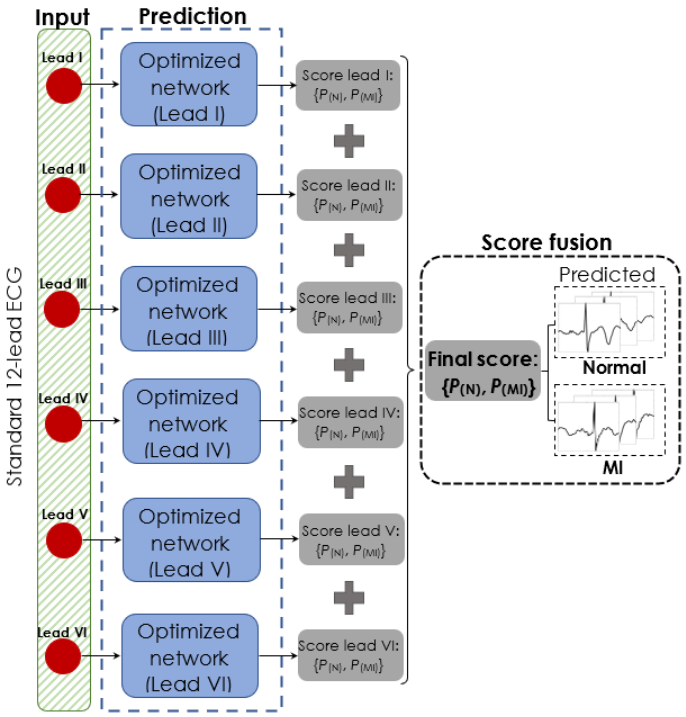

Figure 3 Prediction networks and score fusion strategy

3.0 RESULTS AND DISCUSSION

The test set is composed of 984 ECG pulses from each lead. These data have no role in the network optimization and training process shown in Figure 2 and the steps detailed in Algorithm 1, and they are not a part of the validation set. The testing classification result from the six limb leads I-VI networks is shown in Figure 4. Figure 5 shows the confusion matrix from fusing the scores from different leads in Figure 4. The average inference time for each testing ECG data is timed as 8 ms on an i7-1165G7 CPU with 8Gb RAM.

Based on the results in Figures 4 and 5, the classification performance of the limb networks and fusion strategy is evaluated using the formula of accuracy (*Acc*), sensitivity (*Sens*), specificity (*Spec*), balanced accuracy (*BAcc*), precision (*Prec*), and f1-score (*F1*) expressed in Eq. (2)-(7). The calculated performance metrics (in percentage value) are shown in Table 2. A comparison with prior literature that used the same dataset is in Table 3. Since the prior works in [17,22,23] adopted manual method in developing a 1D network for the same problem, repeating their past successful experiences adds redundancy to the existing knowledge. Hence, only the automated method is implemented in this study and reported in the table.

$$Acc = \frac{TP+TN}{TP+FP+TN+FN} \quad (2)$$

$$Sens = \frac{TP}{TP+FN} \quad (3)$$

$$Spec = \frac{TN}{TN+FP} \quad (4)$$

$$Prec = \frac{TP}{TP+FP} \quad (5)$$

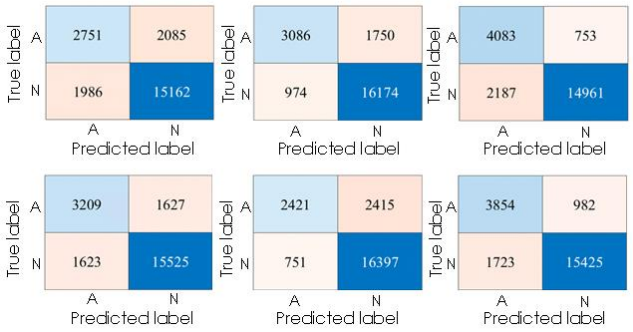

Figure 4 Limb networks classification result. Top: Lead I (left), Lead II (middle), and Lead III (right); bottom: Lead IV (left), Lead V(middle), and Lead VI (right)

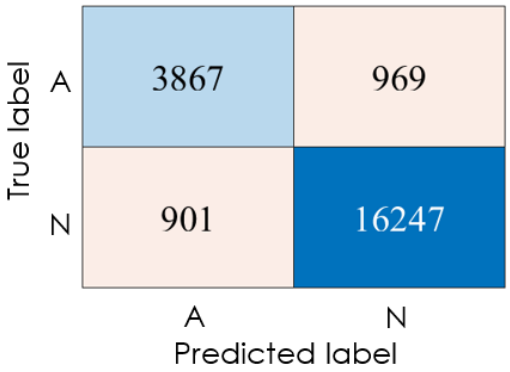

Figure 5 Classification result from all-inclusive system

Table 2 Optimal limb networks parameters and their performance metrics

Network (ECG Lead)	Optimized parameters {*n*, *N*, *α*, *L*, *β*, *γ*}†	Final network weight	Evaluation metrics	
I	10, 12, 2, *Adam*, 1024, 0.0375	8,474,186	*Acc*: 81.5 % *Sens*: 57 % *Spec*: 88.4 %	*Prec*: 58 % *BAcc*: 73 % *F1*: 57.5 %
II	10, 14, 6, *RMSProp*, 809, 0.019	8,479,740	*Acc*: 88 % *Sens*: 64 % *Spec*: 94 %	*Prec*: 76 % *BAcc*: 79 % *F1*: 69 %
III	6, 16, 5, *Sgdm*, 711, 0.0789	8,482,498	*Acc*: 87 % *Sens*: 84 % *Spec*: 87 %	*Prec*: 65 % *BAcc*: 86 % *F1*: 74 %
IV	10, 22, 4, *Adam*, 715, 0.0197	8,504,606	*Acc*: 85.2 % *Sens*: 50.1 % *Spec*: 90.5 %	*Prec*: 66.4% *BAcc*: 70 % *F1*: 57.1 %
V	8, 23, 7, *RMSProp*, 1024, 0.022	8,504,758	*Acc*: 85.6 % *Sens*: 50.1 % *Spec*: 96 %	*Prec*:76.3 % *BAcc*: 72.8% *F1*: 60.5 %
VI	7, 29, 10, *Sgdm*, 562, 0.00252	8,521,814	*Acc*: 87.7 % *Sens*: 80 % *Spec*: 90 %	*Prec*: 69 % *BAcc*: 85 % *F1*: 74 %
Score fusion	-	-	**Acc: 92 %** **Sens: 80 %** **Spec: 94 %**	**Prec: 81 %** **BAcc: 88 %** **F1: 81 %**

† *N*: filter number, *α*: Pooling size, *L*: Learner type, *β*: Minibatch no., *γ*: Initial learning rate

$$BAcc = \frac{Sens+Spec}{2} \quad (6)$$

$$F1 = \frac{2(Prec*Sens)}{Prec+Sens} \quad (7)$$

TP and *TN* are the accurate prediction of MI and normal ECG, respectively. *FN* is the incorrect prediction of MI as normal, whereas *FP* is the misclassification of normal signal as MI class.

The conventional means of MI prediction using a pretrained model, or its cloned version, are computationally expensive and memory intensive, hindering their deployment in critical real-world tasks. It is challenging to design and build a light and efficient network for different tasks. We addressed this problem using the PSO method in our hybrid network design with minimal computing resources. Our findings in Table 2 showed an overall good performance for all lead networks, implying our proposed framework's high flexibility and adaptability. This process produces networks of thin layers with depth in the 12-29 range, as shown in Table 2. These networks are comparatively lightweight, with about 8.5 million trainable parameters as compared to most traditional CNNs, such as AlexNet (with 62 million parameters), ResNet variants (11-58 million), and VGGNets (138-143 million). This significant reduction in the network parameters (by 1.3 – 17 folds) is capable of a great reduce in the computational time by the same fold as widely reported in the literature [28]. The inconsistency in the design parameters' value for each lead network in this table is due to differences in the input dataset containing measurements from different heart locations. These thin deep networks are computationally efficient, with an average inference time of 8 ms, which suggests that they can be used for real-time applications or home-based monitoring where quick and reliable single-lead ECG classification is required.

Based on the comparison results in Table 2, there exists a high consistency in the accuracy performance of systems, with the values ranging between 81-88 %. However, the lead I system performs inferior to the rest. The figures in this table also showed its much poorer sensitivity performance, with a score of 57 %. Since this metric carries information on the misdiagnosis rate of abnormal or MI cases, a high sensitivity score is often desired to allow prompt treatment. In recognizing normal ECG, all the lead networks achieved a high recognition rate with a considerably high specificity rate of around 90 %. We attribute this to the better generalization of the model for normal ECG using the extensive training data of the class. Investigating the

Table 3 Classification performance of Fusion MI-OptNet compared with literature reports using PTB-XL dataset

Investigator	Strategy/model	Accuracy	Balanced accuracy	Sensitivity	Specificity	Precision	f1-score
Proposed Fusion MI-OptNet	Network design optimization/ Score fusion	92 %	88 %	80 %	94 %	81 %	81 %
Strodthoff *et al.* [31]	Transfer learning (TL)/ ResNet	84-85 %	NA	NA	NA	NA	NA
	TL/LSTM	83-84 %	NA	NA	NA	NA	NA
	TL/Ensemble	85 %	NA	NA	NA	NA	NA
	TL/Inception	84 %	NA	NA	NA	NA	NA
Mehari and Strodthoff [32]	TL/ResNet	72-92 %	NA	NA	NA	NA	NA
	multilayer perceptron (MLP) -LSTM	71-93 %	NA	NA	NA	NA	NA
	Self-supervised/ MLP-LSTM	92-94 %	NA	NA	NA	NA	NA
Pałczyński *et al.* [33]	Few shot learning/KNN	88 %	NA	86-87 %	89 %	NA	86-87 %
	Few shot learning/SVM	68-88 %	NA	66-88 %	68-90 %	NA	66-87 %
Zhu *et al.* [22]	Feature elimination/ Own developed 1D CNN	87-89%	NA	87-91 %	NA	87-90 %	87-90 %
Śmigiel *et al.* [17]	Entropy feature/ Own developed 1D CNN	83-91 %	NA	NA	NA	NA	83-91 %
Śmigiel *et al.* [23]	TL/SincNet	85.8%	NA	85.4 %	NA	85.5 %	85.5 %
	Entropy feature/ Own developed 1D CNN	89.2 %	NA	89.3 %	NA	88.9 %	89.1 %

balanced accuracy that factorizes class imbalance revealed an excellent and comparable performance between the lead III and VI networks. Their *BAcc* readings and the high sensitivity rate of 80-84 % suggest that signals from both leads can be used to detect MI. Therefore, these leads should be chosen for future research using a single lead for MI prediction. The elevation in the ST-segment in the lead III signals and abnormal Q-waves in the lead VI signals, as reported in the earlier studies [29,30], are likely the factors most responsible for accurate MI prediction. However, their precision and *F1* score range between 64 – 74 % due to the high misclassification rate of normal ECG as MI remains unsatisfactory. This can be improved by exploring deeper and wider architectural alternatives or increasing the degree of freedom for the system to learn more powerful representations of the inputs. Several other factors have been identified as the possible reasons for compromising the system's performance. Poor ECG signal quality and inconsistent PQRST patterns are the leading causes of most misclassification. In addition, inter and intra-person heartbeat variability is another challenge because a fixed input length is needed to meet the key requirement of neural network models. Noises, or the high-frequency component that the filter has not removed completely, and different R peak intervals aggravate these inconsistencies. All the factors mentioned above affect the splitting process and have an important impact on the feature extraction ability of the model. Although this limitation can be avoided by manually examining each ECG data after the automatic segmentation to remove poor-quality signals from the datasets, this data cleaning process may introduce bias in our results due to the use of optimistic data.

Since different electrodes measured ECG from different heart regions, distortions in one of the leads do not necessarily appear in the others. So, combining the scores from all networks (i.e., Fusion MI-OptNet) achieves 92 % prediction accuracy and the best overall performance improvement with an average increase of 10 %. This system gives better confidence in the predicted results without significant efforts needed in the data cleaning and pre-processing stage. The *f1*-score and precision metric increase are particularly distinct (near 20 %) compared to individual limb networks. A comparison in Table 3 shows obvious superiority in the performance of our framework as compared to the earlier works that used pretrained models [31,32] and binary classifiers [33]. This method also shows competitiveness in performance and efficiency compared to the CNN models derived from domain experts [17,22,23]. Even though model overfitting (to the normal ECG) is identified as the primary cause for the misclassification of MI, compromising the classification precision, sensitivity, and f1-score, ranging between 80-81 % in Table 3, we do not rule out the presence of irrelevant and redundant features extracted from the dataset, which affects the classification performance. This interpretation is supported by the fact that the competing studies in [17,22,23,33] have suggested innovative feature selection strategies to eliminate less relevant features, allowing their proposed model to focus on critical features, leading to the improved obtained results. Such approaches and dataset enhancement techniques might be worth exploring in future research. It must also be acknowledged that the proposed automated framework and the manual network design methods in [17,22,23] approach problem-solving differently (i.e., the former involves statistical and systematic exploration of design space while the latter is an intuitive process based on experiential-knowledge and learning), therefore comparison in terms of computational efficiency between the two techniques is not directly possible.

Our findings open an exciting direction for cost and energy-efficient network design techniques, especially for 1D signal applications. This study chooses MI and normal ECG for demonstration; the proposed strategy can also be implemented for detecting diverse heart diseases from ECG signals, such as irregular heartbeats (i.e., arrhythmias), fibrillation and tachycardia, by including their datasets in the training process. Some possible future directions worth pursuing include implementing a fully automated and unsupervised pipeline approach involving several steps, from data segmentation and cleansing to automatic architecture exploration and joint optimization of network design and training processes. Others include the opportunity for field experiments or home-based care using a computationally efficient single-lead ECG system.

4.0 CONCLUSION

While there have been considerable efforts in the past to identify the best strategy for ECG classification, they mostly rely on a computation-heavy pretrained model. Thus, their practical implementation remains a major problem. In this paper, we demonstrated the efficiency of the proposed MI-OptNet using the PSO algorithm in designing a light and effective CNN-LSTM model for identifying MI ECG signals. We showed that our strategy produces a network that gives considerably good classification performances even with the minimal degree of freedom of the problem in our design process. We recommend leads III and VI as the best ECG leads for monitoring MI. Our findings also revealed that using score fusion that combines probability outputs from all considered leads enhances the confidence of our estimates without tedious signal pre-processing. This research is important and can be the start of exciting new ventures in this domain in the future, especially for signal-related deep-learning tasks. A straightforward approach like ours may also be adopted and used in other scientific fields for exploratory research and decision-making tasks.

Conflicts of Interest

The authors declare that there is no conflict of interest regarding the publication of this paper.

Acknowledgement

This research was supported by Universiti Tun Hussein Onn Malaysia (UTHM) through Tier 1 (Q381) and Ministry of Higher Education (MOHE) through Fundamental Research Grant Scheme (FRGS) (FRGS/1/2020/TK0/UTHM/02/28).

References

[1] World Health Organization. 2019. WHO Reveals Leading Causes of Death and Disability Worldwide 2000-2019. [Online] Available at https://www.who.int/news/item/09-12-2020-who-reveals-leading-causes-of-death-and-disability-worldwide-2000-2019.html [Accessed on 28 June 2023].

[2] Centers for Disease Control and Prevention. 2022. Myocarditis and Pericarditis After mRNA COVID-19 Vaccination. [Online] Available at https://www.cdc.gov/coronavirus/2019-ncov/vaccines/safety/myocarditis.html [Accessed on 12 June 2023].

[3] Schneider, R. R., & Seckler, S. G. 1981. Evaluation of Acute Chest Pain. *Med. Clin. N.* 65(1): 53-66. Doi: https://doi.org/10.1016/S0025-7125(16)31539-5.

[4] Ghani, F., Wu, A. H. B., Graff, L., Petry, C., Armstrong, G., Prigent, F., Brown, M. 2000. Role of Heart-Type Fatty Acid-binding Protein in Early Detection of Acute Myocardial Infarction, *Clin. Chem.* 46(5): 718-719. Doi: https://doi.org/10.1093/clinchem/46.5.718.

[5] Feng, Y., Geng, S., Chu, J., Fu, Z., & Hong, S. 2022. Building and Training a Deep Spiking Neural Network for ECG Classification. *Biomed. Signal Process Control*. 77(103749). Doi: https://doi.org/10.1016/j.bspc.2022.103749.

[6] Xu, P., Liu, H., Xie, X., Zhou, S., Shu, M., & Wang Y. 2022. Interpatient ECG Arrhythmia Detection by Residual Attention CNN. *Comput. Math. Methods Med*. 2022: 1-13. Doi: https://doi.org/10.1155/2022/2323625.

[7] Chatterjee, S., Thakur, R. S., Yadav, R. N., Gupta, L., & Raghuvanshi, D. K. 2020. Review of Noise Removal Techniques in ECG Signals. *IET Signal Process*. 14(9): 569-590. Doi: https://doi.org/10.1049/iet-spr.2020.0104.

[8] Xu, B., Liu, R., Shu, M., Shang, X., & Wang, Y. 2021. An ECG Denoising Method based on the Generative Adversarial Residual Network. *Comput. Math. Methods Med*. 2021: 1-23. Doi: https://doi.org/10.1155/2021/5527904.

[9] Ma, S., Cui, J., Xiao, W., & Liu, L. 2022. Deep Learning-based Data Augmentation and Model Fusion for Automatic Arrhythmia Identification and Classification Algorithms. *Comput. Intell. Neurosci*. 2022: 1-17. Doi: https://doi.org/10.1155/2022/1577778.

[10] Ingale, M., Cordeiro, R., Thentu, S., Park, Y., & Karimian, N. 2020. ECG Biometric Authentication: A Comparative Analysis. *IEEE Access*. 8: 117853-117866. Doi: https://doi.org/10.1109/ACCESS.2020.3004464.

[11] Hamil, H., Zidelmal, Z., Azzaz, M. S., Sakhi, S., Kaibou, R., Djilali, S., & Abdeslam, D. O. 2022. Design of a Secured Telehealth System based on Multiple Biosignals Diagnosis and Classification for IoT Application. *Expert Syst*. 39(4): 1-27. Doi: https://doi.org/10.1111/exsy.12765

[12] Chang, R. K. 2022. Resting 12-lead ECG Tests Performed by Patients at Home Amid the COVID-19 Pandemic — Results from the First 1000 Patients. *J. Electrocardiol*. 73(2022): 108-112. Doi: https://doi.org/10.1016/j.jelectrocard.2022.06.006.

[13] Al Rahhal, M. M., Bazi, Y., AlHichri, H., Alajlan, N., Melgani, F. & Yager, R. R. 2016. Deep Learning Approach for Active Classification of Electrocardiogram Signals. *Inf. Sci. (NY)*. 345: 340-354. Doi: https://doi.org/10.1016/j.ins.2016.01.082.

[14] Li, W., Tang, Y. M., Yu, K. M., & To, S. 2022. SLC-GAN: An Automated Myocardial Infarction Detection Model based on Generative Adversarial Networks and Convolutional Neural Networks with Single-lead Electrocardiogram Synthesis. *Inf. Sci. (NY)*. 589: 738-750. Doi: https://doi.org/10.1016/j.ins.2021.12.083.

[15] Rai, H. M., & Chatterjee, K. 2022. Hybrid CNN-LSTM Deep Learning Model and Ensemble Technique for Automatic Detection of Myocardial Infarction using Big ECG Data. *Appl. Intell*. 52: 5366-5384. Doi: https://doi.org/10.1007/s10489-021-02696-6.

[16] Park, Y., Yun, I. D., & Kang, S. H. 2019. Preprocessing Method for Performance Enhancement in CNN-based STEMI Detection from 12-lead ECG. *IEEE Access*. 7: 99964-99977. Doi: https://doi.org/10.1109/ACCESS.2019.2930770.

[17] Śmigiel, S., Pałczyński, K., & Ledziński, D. 2021. Deep Learning Techniques in the Classification of ECG Signals using R-peak Detection based on the PTB-XL Dataset. *Sensors*. 21(8174): 1-18. Doi: https://doi.org/10.3390/s21248174.

[18] Bassiouni, M., Hegazy, I., Rizk, N., El-Dahshan, S. A., & Salem, A. M. 2022. Deep Learning Approach based on Transfer Learning with Different Classifiers for ECG Diagnosis. *Int. J. Intell. Comput. Inf. Sci*. 22(2): 44-62. Doi: https://doi.org/10.21608/ijicis.2022.105574.1137.

[19] Kavak, S., Chiu, X. D., Yen, S. J., & Chen, M. Y. C. 2022. Application of CNN for Detection and Localization of STEMI using 12-lead ECG Images. *IEEE Access*. 10: 38923-38930. Doi: https://doi.org/10.1109/ACCESS.2022.3165966.

[20] Manimekalai, K., & Kavitha, A. 2020. Deep Learning Methods in Classification of Myocardial Infarction by Employing ECG Signals. *Indian J. Sci. Technol*. 13(28): 2823-2832. DOI: https://doi.org/10.17485/IJST/v13i28.445.

[21] Fatimah, B., Singh, P., Singhal, A., Pramanick, D., Pranav, S., & Pachori, R. B. 2021. Efficient Detection of Myocardial Infarction from Single Lead ECG Signal. *Biomed. Signal Process Control*. 68: 1-14. Doi: https://doi.org/10.1016/j.bspc.2021.102678.

[22] Zhu, J., Lv, J., & Kong, D. 2022. CNN-FWS: A Model for the Diagnosis of Normal and Abnormal ECG with Feature Adaptive. *Entropy*. 24(471): 1-13. Doi: https://doi.org/10.3390/e24040471.

[23] Śmigiel, S., Pałczyński, K., & Ledziński, D. 2021. ECG Signal Classification using Deep Learning Techniques based on the PTB-XL Dataset. *Entropy*. 23(1121): 1-20. Doi: https://doi.org/10.3390/e23091121.

[24] Gaziano, T., Reddy, K. S., Paccaud, F., Horton, S., & Chaturvedi, V. 2006. *Disease Control Priorities in Developing Countries*. 2nd ed. New York: Oxford University Press.

[25] Gursoy, H. T., Dereagzi, S. F., Caliskan, U., Dogru, C. Y., Kulekci, F., Kaplan, Z., Bahtiyar, B., Al, A., & Ozeke, O. 2021. An Electrocardiographic Clue for Pseudo-myocardial Infarction due to Arterial Pulse–tapping Artifact: Aslanger's Sign. *J. Innov. Card. Rhythm Manag*. 12: 4685-4687. Doi: https://doi.org/10.19102/icrm.2021.120904.

[26] Pandey, R. K., Dahiya, A. K., Pandey, A. K., & Mandal, A. 2022. Optimized Deep Learning Model Assisted Pressure Transient Analysis for Automatic Reservoir Characterization. *Pet Sci Technol*. 40(6): 659-677. Doi: https://doi.org/10.1080/10916466.2021.2007122.

[27] Naseri, H., Waygood, E. O. D., Wang, B., & Patterson, Z. 2023. Interpretable Machine Learning Approach to Predicting Electric Vehicle Buying Decisions. *Transp. Res. Rec*. 1-14. Doi: https://doi.org/10.1177/03611981231169533.

[28] Lee, K. S., Lee, E., Choi, B., & Pyun, S. B. 2021. Automatic Pharyngeal Phase Recognition in Untrimmed Videofluoroscopic Swallowing Study Using Transfer Learning

with Deep Convolutional Neural Networks. *Diagnostics*. 11(2): 1-15. Doi: https://doi.org/10.3390/diagnostics11020300

[29] Al-Mansouri, L. A., Al-Obaidi, F. R., & Raheem Al-Humrani, A. H. 2019. Higher ST-Segment Elevation in Lead III than Lead II in Acute Inferior Myocardial Infarction can be a Predictor of Short-term Morbidity and Mortality. *Iraqi J. M. S*. 17(3&4): 168-174. Doi: https://doi.org/10.22578/IJMS.17.3-4.2.

[30] Islam, M., Bhattacharjee, B., Chowdhury, M., Siddique, A. N., & Rezaul Karim, A. M. 2016. Outcome of Acute Myocardial Infarction Patients Admitted in a Tertiary. *Med. Today*. 28(1): 6-8. Doi: https://doi.org/10.3329/medtoday.v28i1.30960.

[31] Strodthoff, N., Wagner, P., Schaeffter, T., & Samek, W. 2021. Deep Learning for ECG Analysis: Benchmarks and Insights from PTB-XL. *IEEE J. Biomed. Heal. Informatics*. 25: 1519-1528. Doi: https://doi.org/10.1109/JBHI.2020.3022989.

[32] Mehari T., & Strodthoff, N. 2022. Self-supervised Representation Learning from 12-lead ECG Data. *Comput. Biol. Med*. 141(105114): 1-15. Doi: https://doi.org/10.1016/j.compbiomed.2021.105114.

[33] Pałczyński, K., Śmigiel, S., Ledziński, D., & Bujnowski, S. 2022. Study of the Few-Shot Learning for ECG classification based on the PTB-XL dataset. *Sensors*. 22(3): 1-25. Doi: https://doi.org/10.3390/s22030904.